Augmenting coarse-grid 3D CSEM with data from a towed-receiver array

Jan Petter Morten*, Jean-Michael Poudroux, and Rune Mittet, EMGS ASA

SUMMARY

We consider the simultaneous 3D CSEM inversion of data from a towed receiver array and a very coarse grid of stationary seabed receivers. The inversion results show that the short-offset data from the towed receivers are effective at resolving a shallow resistor along the towlines. On the other hand, the data from the stationary seabed receivers have less noise and will resolve the 3D geometry of deeper resistive structure typical for a hydrocarbon reservoir. We discuss uncertainty contributions in the two receiver types, and contaminated the synthetic data with noise corresponding to realistic levels.

INTRODUCTION

The data from seabed receivers used in 3D CSEM surveys can effectively resolve subsurface resistivity structure due to *e.g.* hydrocarbon accumulations, lithology, and salt. When the survey is acquired in frontier areas, the definition of prospects can be uncertain, or the survey may be intended to generate prospects related to larger hydrocarbon reservoirs. Cost-effective coarse receiver grids can be used in such surveys to cover large areas. While giving good definition of deeper structure, such coarse receiver grids result in limited short-offset data which is important to define shallow resistors.

Towed receiver systems that can be deployed in conjunction with a horizontal electric dipole source have recently been developed (Constable et al., 2012). The fixed-offset data from such receivers towed behind the vessel have been used for *e.g.* 2D mapping of shallow gas hydrates (Weitemeyer and Constable, 2010). The operational complexity of towing such equipment close to the seafloor typically limits the offset range, but the data could be very useful to complement the coarse-grid 3D CSEM survey technique described above.

In this paper we consider 3D inversion of CSEM data from a towed receiver array as well as stationary seabed receivers. We invert synthetic data that have been contaminated by noise at realistic levels. The model considered contains targets representing typical hydrocarbon reservoirs at various burial depths, as well as a large-scale very shallow thin resistor. The inversions are carried out using either data from the towed or stationary receivers alone, or we include data from both receiver types in combination. We discuss the effect on imaging for the three data combinations, and discuss the uplift from complementing the coarse-grid 3D CSEM survey data with towed-receiver data.

NOISE MODEL

In order to assess the potential imaging improvement from towed receiver data, it is important that the synthetic data real-

istically reflects the noise levels which can be achieved in acquisition. We will now describe the noise model which is used to contaminate the synthetic responses to be input to inversion.

The noise in marine CSEM data can be classified as either ambient noise or constituting a relative uncertainty (Mittet and Morten, 2012). The ambient noise describes effects due to *e.g.* magnetotelluric signals, noise from receiver motion and ocean swell, and receiver electronics. This type of noise would be present in the data even though the source was not transmitting. The relative uncertainty contributions depend on the magnitude of the source dipole moment, and describe the effect from fluctuations in *e.g.* source position or source current amplitude, as well as corresponding uncertainty in receiver positioning and sensor calibration.

The contamination of data with noise is done according to an approximation discussed in Mittet and Morten (2012),

$$E_i\left(\mathbf{r}|\mathbf{r}', \omega\right) \rightarrow (1+\alpha)E_i\left(\mathbf{r}|\mathbf{r}', \omega\right) + \eta(\omega). \quad (1)$$

In this expression, $E_i(\mathbf{r}|\mathbf{r}', \omega)$ is the electric field component i at position $\mathbf{r}$ due to a unit dipole source at position $\mathbf{r}'$ operating at angular frequency ω. The relative uncertainty and ambient noise contributions are modeled by α and η respectively. These quantities are complex random variables with Gaussian distributed (Myer et al., 2012) real and imaginary parts of mean zero and standard deviations $\delta\alpha/\sqrt{2}$ and $\delta\eta/\sqrt{2}$. The factor α is dimensionless, and η has the unit V/m. The ambient noise standard deviation typically varies with frequency, but in this paper we will consider a simplified situation where the standard deviation is a constant.

Motion noise effects arise whenever the sensor equipment is moving in the environment of the conductive seawater and the earth magnetic field. We expect that such contributions will be significantly higher for towed receivers moving through the seawater than stationary seabed receivers which can be designed to minimize movement from seabed position, see *e.g.* experimental data in Constable et al. (2012). In this paper we consider the electric field from a finite-length (270 m) dipole source of unit dipole moment 1 Am, and we will utilize the noise value $\delta\eta_{\text{seabed}} = 10^{-16}$ V/m for stationary seabed receivers, and $\delta\eta_{\text{towed}} = 10^{-15}$ V/m for towed receivers. Note that our setup with these numerical values is equivalent to considering normalized data but with units V/Am^2 instead.

Contributions to the relative uncertainty factor from any fluctuations in source parameters will similarly affect both stationary seabed and towed receivers. However, the data from towed receivers will suffer from larger effects of navigation uncertainty due to the less accurate dynamical positioning and fluctuations in receiver position during signal transmission. The position and orientation of the stationary receivers can be determined very accurately by stacking many independent measurements of their position. To obtain a quantitative measure for $\delta\alpha$ we use the error propagation techniques described in Mittet and

Morten (2012). Error propagation can determine the aggregate uncertainty from the sum of equipment-characteristic properties like the fluctuation in *e.g.* offset, orientation, and calibration on a single receiver.

Mittet and Morten (2012) describes an equipment setup for stationary seabed receivers which results in $\delta\alpha_{\mathrm{seabed}} = 0.03$. This setup is characterized by relative fluctuations in source current, source dipole length, and receiver calibration all on the scale of 1 %. Further, for the source the uncertainty in the pitch orientation angle is $\pm 1°$. The positioning uncertainty for the source-receiver system in the towing direction is ± 15 m and in the vertical direction it is ± 5 m. This parameter setup is characteristic of CSEM equipment commonly used today, and will be assumed for the stationary receiver data in this paper.

We now consider the relative uncertainty for towed receiver data, $\delta\alpha_{\mathrm{towed}}$. We assume the same uncertainty parameters for the source, but fluctuations in the positioning and orientation of the towed receivers will give a larger total uncertainty. For the short-offset data considered here, Mittet and Morten (2012) also show that the relative uncertainty is particularly sensitive to errors in the source-receiver offset, and that the magnitude is offset-dependent. At close offset, the uncertainty increases with decreasing offset due to a term proportional to the derivative of the field strength in the inline direction. On the other hand, for the towed receivers we expect that the source-receiver offset uncertainty will increase with the length of the towing cable, as well as the tow speed. In this paper we make the simplifying assumption that $\delta\alpha_{\mathrm{towed}}$ can be approximated as a constant for the limited offset range considered. Assuming that the source-receiver offset fluctuations are the dominating contribution to the uncertainty, and that for the towed-receiver configuration the uncertainty is ± 30 m we estimate the value $\delta\alpha_{\mathrm{towed}} = 0.06$ within the approximations assumed.

In order to illustrate the effect of the noise on the towed receiver data, we show in Figure 1 the inversion input data responses from one towline. The towed receiver data at 3.2 Hz for the different offsets are color-coded, and the responses are plotted at the source-receiver common mid-point (CMP) position. For the offsets considered in this paper, the data amplitudes are significantly larger than the ambient noise level $\delta\eta_{\mathrm{towed}}$ for all frequencies included. Even at the farthest offset (3 km) and highest frequency (3.2 Hz), the signal-to-noise ratio is close to 10. Thus the fluctuations in the data shown in Figure 1 are due to the relative uncertainty contribution.

SURVEY LAYOUT AND DATA SENSITIVITY

We will consider the inversion of synthetic data from the survey layout illustrated in Figure 2. The dataset has in total 12 source towlines in two orthogonal directions named *x* and *y*. The source is towed at constant elevation 30 m above the seabed, and the water depth is 1 km. The 36 stationary seabed receivers record the horizontal components of the electric and magnetic field for all the source towlines. The spacing between the seabed receiver stations is $L = 2.9$ km, and source positions for these receivers were simulated at 100 m intervals
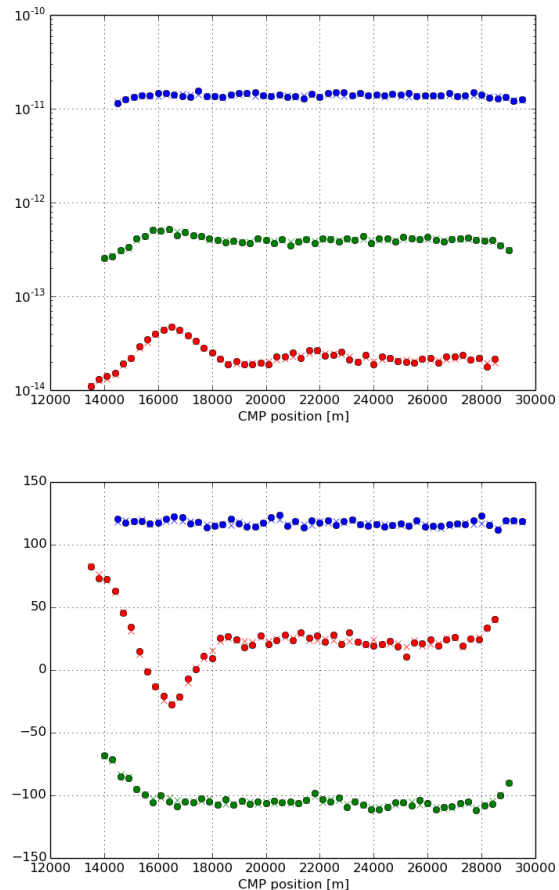

Figure 1: Towed receiver amplitude (top) and phase (bottom) data at 3.2 Hz for cross-section 1-1' (see Figure 2) plotted at CMP position along the towline. Color coding: Blue 1 km offset, green 2 km offset, red 3 km offsets. The filled circles are the inversion input data obtained by contaminating the synthetic data from the true model with noise according to (1). The crosses represent the corresponding synthetic data from the inversion of the combined dataset with both stationary and towed receivers.

along the towlines. All data points at offsets from 1 km up to 10 km were included unless the magnitude fell below the noise levels specified below.

Along the source towlines we have also simulated data for a towed array of three receivers. The towed receivers are located at fixed-offsets 1.0, 2.0, and 3.0 km behind the source, and at the same elevation as the source. In this paper we have included data for inline electric field recordings at intervals spaced $dL = 300$ m along the towlines for each of the towed receivers.

The source frequencies are the same for both towed receivers and stationary seabed receivers. The simulated acquisition implies that the same source is used for both receiver types. We included frequencies 0.8, 1.3, 2.0, and 3.2 Hz in our dataset. For short offsets, low-frequency data responses will typically
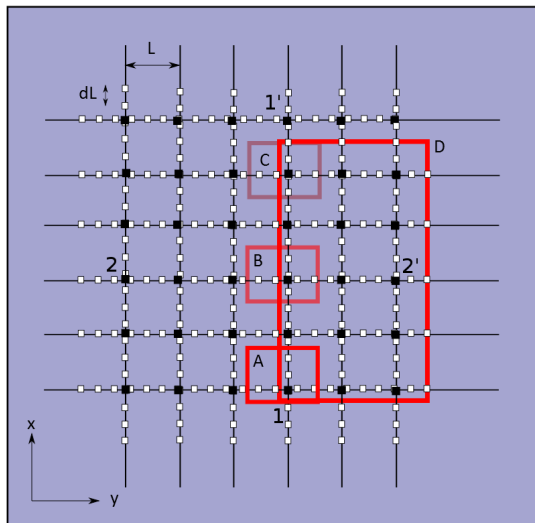
Figure 2: Schematic survey layout and lateral resistor outlines (red). The black and white dots respectively illustrate the stationary seabed and the towed receiver locations. The burial depth is 1000, 1500, 2000, and 400 m for resistors A, B, C, and D respectively. Resistors A, B, and C have resistivity 100 Ωm and measure $3000 \times 5000 \times 100$ m^3. Resistor D has resistivity 10 Ωm and measures $15000 \times 8000 \times 50$ m^3. The towline and stationary receiver spacing is $L = 2900$ m, and the towed receivers have data point separation $dL = 300$ m.

be dominated by direct propagation through seawater or propagation along the seabed (Løseth, 2011), whereas higher frequencies can give valuable information about the shallower parts of the formation even at short offset. In our survey we have therefore chosen to include higher frequencies than might typically considered in a high-conductive background. This will ensure that the towed receiver data has good sensitivity to shallow structure.

We consider a model with a constant water depth of $z_{wd} = 1$ km and homogeneous water conductivity 4 S/m. The total lateral size (x- and y-dimensions) of our model is 44×44 km, and the total depth (z) is 5.0 km. The background resistivity varies with all three coordinates, such that the resistivity just below the seabed is 1.0 Ωm, and the maximum resistivity at approximately 10 Ωm is reached at the largest depth in the uppermost corner of the model. In the present study, we consider an isotropic model.

Four resistors are embedded in our model. The lateral extents of these resistors are indicated in Figure 2. In the figure, the resistors are labeled A, B, C, and D. The three targets A, B, C represent typical hydrocarbon reservoirs at various burial depths 1.0, 1.5, 2.0 km below the seabed. The thicknesses and resistivities of these targets are identical and equal to 100 m and 100 Ωm. The resistor D represents a regional shallow feature and is buried 400 m below the seabed. Resistor D has lower thickness and resistivity than the targets. The thickness of resistor D is 50 m and its resistivity is 10 Ωm. The lateral extent of targets A, B, and C is 3×5 km. Resistor D is much

larger 15×8 km and has a partial lateral overlap with all the targets.

The offset variation seen in Figure 1 can be correlated to target positions and demonstrates the sensitivity of the towed receiver data. Comparing to the position along the profile 1-1' in Figure 2 we see that the target A has a clear impact on the data especially for the towed receivers at 2 km and 3 km offsets. The shortest source-receiver offset 1 km has low target sensitivity due to the dominating contribution from the direct-wave. The direct-wave signals are determined by propagation only through the water and has no sensitivity to the resistivity distribution below the seafloor. Further, the data responses from the deeper targets B and C constitute small effects on the scale of the measurement error or less at all the towed receiver offsets. The towed receiver data has good sensitivity towards the shallow resistor D, as seen from the impact on the data at the resistor termination close to the end of the profile. The lower frequencies in the dataset have similar qualitative features as the data shown in the figure, but the relative resistor responses are weaker (not shown).

INVERSION RESULTS

We carried out isotropic 3D inversion for three cases of data selection (1) only data from seabed receivers (2) only data from towed receivers, and (3) combined dataset with both seabed and towed receivers. We utilize the limited-memory BFGS optimizer described in Zhu et al. (1997) and a finite-difference time-domain forward solver described in Maaø (2007). The number of data points from the seabed receivers, N_{seabed}, will be much larger than the number of data points from the towed receivers, N_{towed}. This is due to the fact that the seabed receivers record signals not only from the source towline crossing over the receiver position, but also from all the other towlines where the source generates a signal above the noise level. For the survey shown in Figure 2 we had $N_{seabed}/N_{towed} \approx 33$. To balance the influence of the two data types in the inversion cost function, we normalize each data type contribution by the number of samples,

$$\varepsilon_{Data} = \frac{1}{N_{seabed}} \varepsilon_{seabed} + \frac{1}{N_{towed}} \varepsilon_{towed}, \qquad (2)$$

where the cost function terms in this expression are computed using the $L2$ norm. The data weights for inversion was calculated using the standard deviations of α and η of the noise model in Eq. (1). We also include a total variation regularization term in the cost function which acts to smooth the reconstruction laterally.

All inversions shown converged on a model where the misfit was on the scale of the noise added to the data. Figure 1 illustrates this for the case where we inverted both the towed receiver data and the seabed receiver data. Cross-sections along the profile 1-1' indicated in Figure 2 are shown in Figure 3. More details regarding the inversion result and input data can be found in Morten et al. (2014).

Let us now discuss the imaging results shown in Figure 3. The seabed receivers have good sensitivity towards the shallow re-

(a) Seabed receivers

(b) Towed receivers

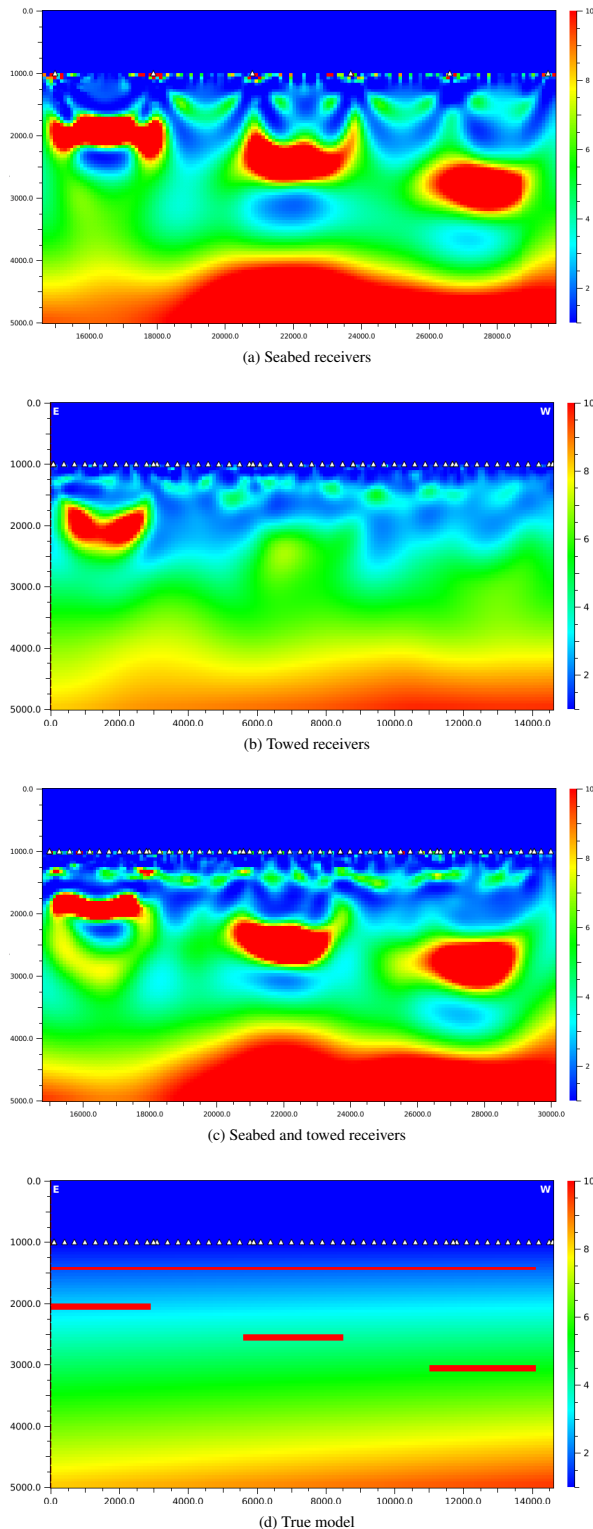(c) Seabed and towed receivers

(d) True model

Figure 3: Inversion result cross-sections along the towline marked 1-1' in Figure 2: (a) only data from seabed receivers, (b) only data from towed receivers, (c) using data from both seabed and towed receivers, (d) true model. Color scale shows resistivity in Ωm.

sistor D, but the imaging results is poor. The result in panel (a) shows a partial reconstruction as thick resistive zones broken up at receiver positions. The reason for the poor imaging of resistor D is a result of the lack of short-offset information. The imaging of the shallow resistor D achieved from the towed receiver data alone shows a much more realistic reconstruction in terms of the thickness and continuity. The spatial inhomogeneity is related to the noise added to the data. When we combine the data from seabed and towed receivers, the inversion result in Figure 3 (c) shows that the complementary sensitivity leads to a much improved imaging result for resistor D. The imaging improvement is, however, most apparent at cross-sections coinciding with a towline. The 2D nature of the data coverage from the towed receiver array gives limited sensitivity towards structure off towlines (not shown).

Let us now consider the imaging results for the deeper targets A,B, and C. The inversion result obtained from the seabed receivers, Figure 3 (a), resolved all the deep targets with the approximate correct transverse resistance and depth. The geometry of the shallowest target A is somewhat distorted due to the limited sampling of the sparse receiver grid. The thickness resolution for target C is not as good as for target A. This is because the higher frequencies are less sensitive to the deepest target due to signal attenuation in the conductive overburden. As we can see from the result shown in Figure 3 (b), the towed receiver data lacks sensitivity to the deeply buried targets B and C. This is due to the limited offset range of the towed receiver array, but also the higher noise levels. However, the result achieved when combining the datasets shown in Figure 3 (c), preserves resolution of the deep targets from the seabed receiver data, along with the improved shallow resistor imaging from towed receiver data.

CONCLUSIONS

Cost-effective, coarse-grid 3D CSEM can be deployed for frontier exploration. We considered augmenting such surveys with data from an array of receivers towed at fixed offsets behind the source. The towed receiver array data is acquired at the same time as the stationary seabed receiver data is acquired, such that the additional vessel time used for the survey is small. In our synthetic study, we utilize a noise model that reflects the operational character of the different equipment sets. The noise contributions proportional to the source dipole moment dominate over ambient noise for the towed receiver data in this study. Our 3D inversion results show that the data from the towed receiver array is useful to improve shallow resistor imaging and can significantly enhance the imaging result.

ACKNOWLEDGMENTS

EDITED REFERENCES

Note: This reference list is a copyedited version of the reference list submitted by the author. Reference lists for the 2015 SEG Technical Program Expanded Abstracts have been copyedited so that references provided with the online metadata for each paper will achieve a high degree of linking to cited sources that appear on the Web.

REFERENCES

Constable, S., P. Kannberg, K. Callaway, and D. R. Mejia, 2012, Mapping shallow geological structure with towed marine CSEM receivers: 82nd Annual International Meeting, SEG, Expanded Abstracts, doi:10.1190/segam2012-0839.1.

Løseth, L. O., 2011, Insight into the marine controlled-source electromagnetic signal propagation: Geophysical Prospecting, **59**, no. 1, 145–160, http://dx.doi.org/10.1111/j.1365-2478.2010.00898.x.

Maaø, F., 2007, Fast finite-difference time-domain modeling of marine-subsurface electromagnetic problems: Geophysics, **72**, no. 2, A19–A23, http://dx.doi.org/10.1190/1.2434781.

Mittet, R., and J. Morten, 2012, Detection and imaging senstivity of the marine CSEM method: Geophysics, **77**, no. 6, E411–E425, http://dx.doi.org/10.1190/geo2012-0016.1.

Morten, J. P., J.-M. Poudroux, and R. Mittet, 2014, Augmenting coarse-grid 3D CSEM with data from a towed-receiver array: Submitted for publication in Geophysics.

Myer, D., S. Constable, K. Key, M. Glinsky, and G. Liu, 2012, Marine CSEM of the Scarborough gas field, Part 1: Experimental design and data uncertainty: Geophysics, **77**, no. 4, E281–E299, http://dx.doi.org/10.1190/geo2011-0380.1.

Weitemeyer, K., and S. Constable, 2010, Mapping shallow geology and gas hydrate with marine CSEM surveys: First Break, **28**, no. 6.

Zhu, C., R. H. Byrd, P. Lu, and J. Nocedal, 1997, Algorithm 778: L-BFGS-B: FORTRAN routines for large-scale bound, constrained optimization: ACM Transactions on Mathematical Software (TOMS), **23**, no. 4, 550–560, http://dx.doi.org/10.1145/279232.279236.